Volume 218 October 2014 ISSN 0022-4596

ELSEVIER

JOURNAL OF SOLID STATE CHEMISTRY

IN THIS ISSUE:

Pronounced matrix effect in $YbMo_2Al_4$-type $Ca(Au_xZn_{2-x})Au_4$ (x=0.09–0.89)

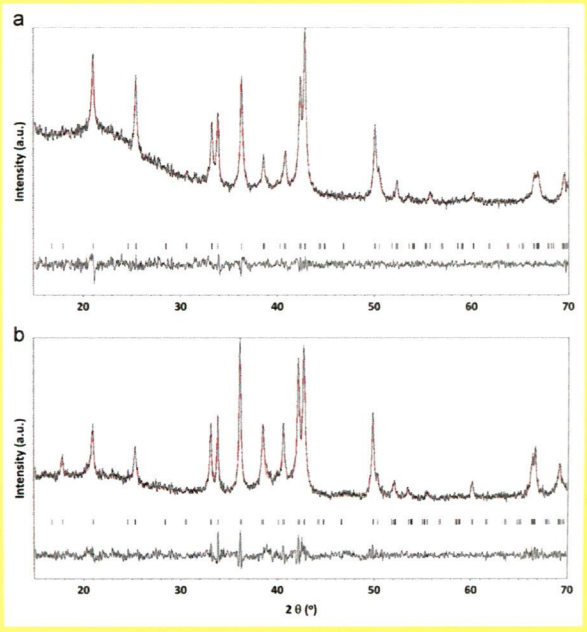

Trinath Mishra, Qisheng Lin and John D. Corbett

ELSEVIER

Volume 218, October 2014

CONTENTS

JOURNAL OF SOLID STATE CHEMISTRY

www.elsevier.com/locate/jssc

Abstracted/indexed in BioEngineering Abstracts, Chemical Abstracts, Coal Abstracts, Current Contents/Physics, Chemical, & Earth Sciences, Engineering Index, Research Alert, SCISEARCH, Science Abstracts, and Science Citation Index. Also covered in the abstract and citation database SCOPUS®. Full text available on ScienceDirect®.

Regular Articles

The influence of pressure on the structure of a 2D uranium(VI) carboxyphosphonoate compound
Elinor C. Spencer, Nancy L. Ross, Robert G. Surbella III and Christopher L. Cahill
page 1

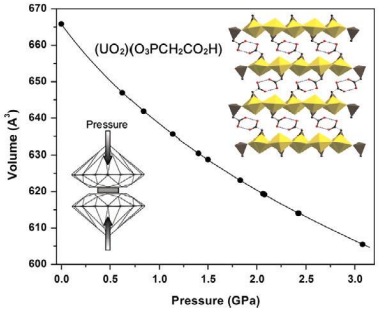

The compression mechanism and elastic constants for a 2D Uranium(VI) carboxyphosphonoate compound are reported.

Two isostructural layered oxohalide compounds containing Mn^{2+}, Te^{4+} and Si^{4+}; crystal structure and magnetic susceptibility
Iwan Zimmermann, Reinhard K. Kremer and Mats Johnsson
page 6

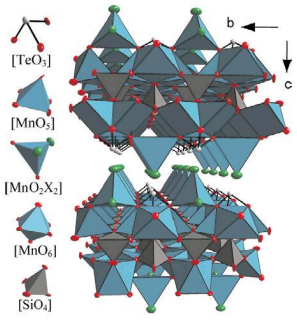

The new compounds $Mn_4(TeO_3)(SiO_4)X_2$ (X=Br, Cl) are layered with weak Van der Waal interactions in between the layers. Manganese adopts various distorted coordination polyhedral, other building blocks are $[SiO_4]$ tetrahedra and $[TeO_3]$ trigonal pyramids. Magnetic susceptibility measurements indicate antiferromagnetic ordering at low temperatures and a large frustration parameter.

Regular Articles—Continued

The molten hydrated flux synthesis of a novel open-framework copper borophosphate and its structural relation with the precursors
Long Zhao, Wei Liu, Xiaohong Ma, Lixin Cao, Ge Su and Zhisheng Lu
page 10

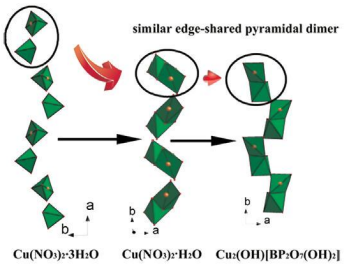

Structure comparison of $Cu(NO_3)_2 \cdot 3H_2O$, $Cu(NO_3)_2 \cdot H_2O$ and $Cu_2(H_2O)[BP_2O_7(OH)]$, showing the structural evolution of CuO_5 pyramids in the synthetic process.

Phase transition, crystal water and low thermal expansion behavior of $Al_{2-2x}(ZrMg)_xW_3O_{12}{\cdot}n(H_2O)$
Fang Li, Xiansheng Liu, Wenbo Song, Baohe Yuan, Yongguang Cheng, Huanli Yuan, Fuxing Cheng, Mingju Chao and Erjun liang
page 15

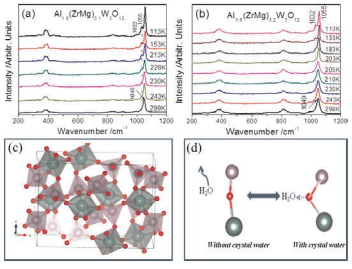

(a and b) Temperature dependent Raman spectra of $Al_{2-x}(ZrMg)_xW_3O_{12}$ (x=0.1, 0.2), (c and d) Building block of a unit cell of $Al_{2-x}(ZrMg)_xW_3O_{12}{\cdot}n(H_2O)$ and schematic showing the effect of crystal water on Al(Zr, Mg)–O–W linkages.

Continued

Syntheses, crystal structures, and characterization of three 1D, 2D and 3D complexes based on mixed multidentate N- and O-donor ligands
Huai-Xia Yang, Zhen Liang, Bao-Lian Hao and Xiang-Ru Meng
page 23

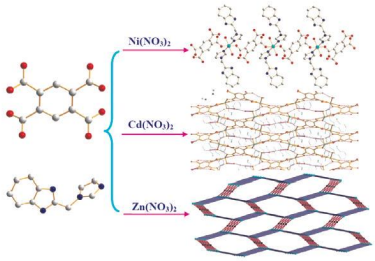

Three new 1D to 3D complexes with different structural and topological motifs have been obtained by modifying the central metal ions. Additionally, their IR, TG analyses and fluorescent properties are also investigated.

Experimental and theoretical methods to study structural phase transition mechanisms in $K_3WO_3F_3$ oxyfluoride
A.S. Krylov, S.N. Sofronova, E.M. Kolesnikova, Yu.N. Ivanov, A.A. Sukhovsky, S.V. Goryainov, A.A. Ivanenko, N.P. Shestakov, A.G. Kocharova and A.N. Vtyurin
page 32

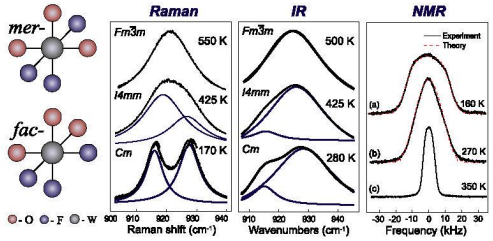

(1) Two possible configuration of octahedra. (2). All phases Raman lines of octahedra. (3) All phases IR lines of octahedra. (4) NMR spectra of all phases.

Crystal structure of brownmillerite Ba_2InGaO_5
Christophe Didier, John Claridge and Matthew Rosseinsky
page 38

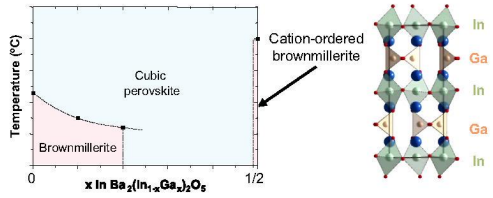

In/Ga cation ordering occurs only for the $x=\frac{1}{2}$ composition in brownmillerite $Ba_2(In_{1-x}Ga_x)_2O_5$. The increased ordering results in an anomalously higher disordering transition temperature to the cubic perovskite.

Mg dopant in Cu_2SnSe_3: An n-type former and a promoter of electrical mobility up to 387 $cm^2\ V^{-1}\ s^{-1}$
Dong-Hau Kuo and Walelign Wubet
page 44

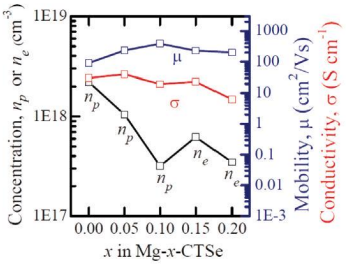

The effects of extrinsic doping of Mg^{2+} on the electrical properties of Cu_2SnSe_3 bulks.

Co(II)-doped MOF-5 nano/microcrystals: Solvatochromic behaviour, sensing solvent molecules and gas sorption property
Ji-Min Yang, Qing Liu and Wei-Yin Sun
page 50

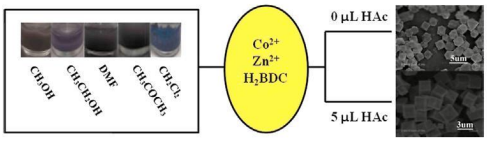

Co(II)-doped MOF-5 nano/microcrystals with different shapes and sizes were synthesized by a facile hydrothermal method, which not only enhance gas sorption properties and structural stability of MOFs towards moisture, but also act as new sensing materials for sensing small molecules.

Synthesis and characterization of mangenese(III) porphyrin supported on imidazole modified chloromethylated MIL-101(Cr): A heterogeneous and reusable catalyst for oxidation of hydrocarbons with sodium periodate
Farnaz Zadehahmadi, Shahram Tangestaninejad, Majid Moghadam, Valiollah Mirkhani, Iraj Mohammadpoor-Baltork, Ahmad R. Khosropour and Reihaneh Kardanpour
page 56

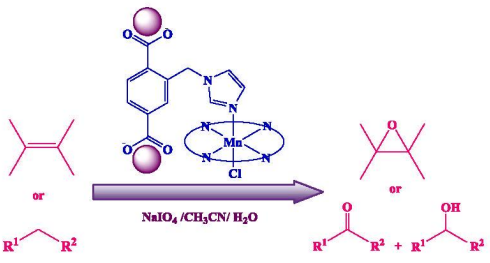

A new carboxyl-copper-organic framework and its excellent selective absorbability for proteins
Linyan Yang, Liangliang Xin, Wen Gu, Jinlei Tian, Shengyun Liao, Peiyao Du, Yuzhang Tong, Yanping Zhang, Rui Lv, Jingyao Wang and Xin Liu
page 64

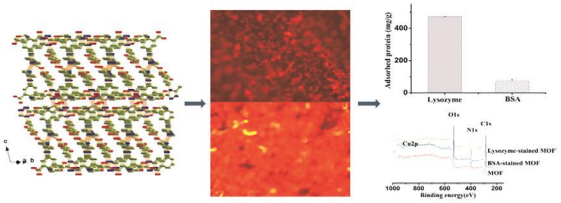

One-pot solvothermal treatments of $CuCl_2{\cdot}2H_2O$, H2L (5-(3-methyl-5-(pyridin-4-yl)-4H-1, 2, 4-triazol-4-yl) isophthalic acid) and $Sm(NO_3)_3{\cdot}6H_2O$ in water yielded a rare carboxyl-copper-organic framework, $[Cu(HL)]n{\cdot}nH_2O$ (1). The existence of carboxyl groups in compound 1 may be due to the interference of $Sm(NO_3)_3{\cdot}6H_2O$ at the relatively high temperature and autogenous pressure of the reaction. Compound 1 has been characterized by single-crystal X-ray diffraction, XRPD, IR, and elemental analysis. Compound 1 is a 3D coordination polymer, and an xfe-4-Fddd, $(4^2.6.8^3)$ topology in 1 is created. In addition, the optical properties have been investigated. Rhodamine B dyeing experiments exhibited that there were residual carboxyl groups on the surface of compound 1. UV-vis results showed that more lysozyme was adsorbed onto the surface of compound 1 than that of BSA at pH 7.4. At the same time, XPS spectra were also investigated to verify the results.

Sulfuric acid functional zirconium (or aluminum) incorporated mesoporous MCM-48 solid acid catalysts for alkylation of phenol with *tert*-butyl alcohol
Tingshun Jiang, Jinlian Cheng, Wangping Liu, Lie Fu, Xuping Zhou, Qian Zhao and Hengbo Yin
page 71

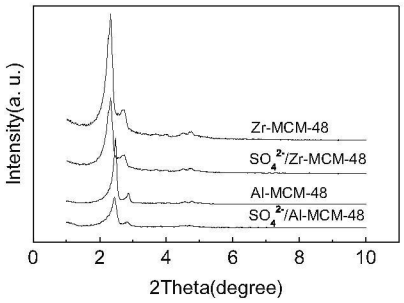

Preparation of highly photocatalytic active CdS/TiO_2 nanocomposites by combining chemical bath deposition and microwave-assisted hydrothermal synthesis
Li Li, Lili Wang, Tianyu Hu, Wenzhi Zhang, Xiuli Zhang and Xi Chen
page 81

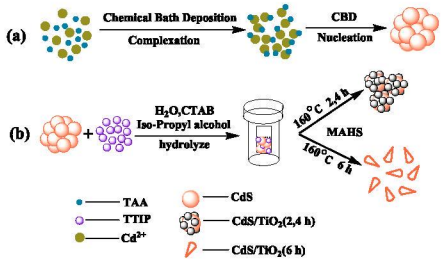

CdS/TiO_2 nanocomposites were prepared using CTAB by CBD combined with MAHS method. In addition, with increasing microwave irradiation time, the morphology of CdS/TiO_2 changed from popcorn-like to wedge-like structure.

Effect of $ZnCl_2$ activation on CO_2 adsorption of N-doped nanoporous carbons from polypyrrole
Long-Yue Meng and Soo-Jin Park
page 90

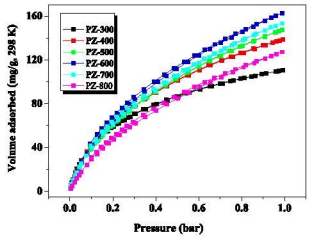

CO_2/298 K adsorption/desorption isotherms of the N-enriched porous carbons.

Phase transitions and hydrogen bonding in deuterated calcium hydroxide: High-pressure and high-temperature neutron diffraction measurements
Riko Iizuka, Kazuki Komatsu, Hiroyuki Kagi, Takaya Nagai, Asami Sano-Furukawa, Takanori Hattori, Hirotada Gotou and Takehiko Yagi
page 95

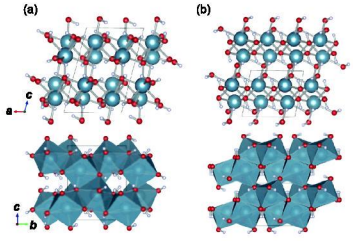

Crystal structures of high-pressure polymorphs of $Ca(OD)_2$, (a) at room temperature (phase II′) and (b) at high temperature (phase II), were obtained from *in situ* neutron diffraction measurements.

Continued

Pronounced matrix effect in $YbMo_2Al_4$-type $Ca(Au_xZn_{2-x})Au_4$ (x=0.09–0.89)
Trinath Mishra, Qisheng Lin and John D. Corbett
page 103

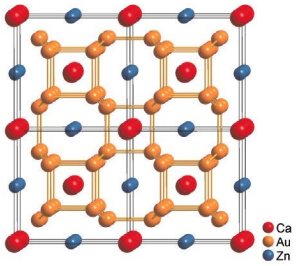

Pronounced matrix effect incurred by Au–Au bonding within the gold substructure in $Ca(Au_xZn_{2-x})Au_4$ results in an elongation of the channel-to-chain Au–Zn interatomic distance without weakening bonding interactions.

Syntheses, crystal and band structures, and optical properties of a selenidoantimonate and an iron polyselenide
Guang-Ning Liu, Wen-Juan Zhu, Ming-Jian Zhang, Bo Xu, Qi-Sheng Liu, Zhen-Wei Zhang and Cuncheng Li
page 109

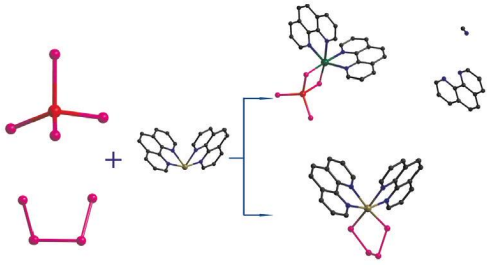

Two metal–Se complexes, representing the only example of a selenidoantimonate ligand to a TM π-conjugated ligand complex, and a tetraselenide ligand to a Fe complex cation, were synthesized.

Oxygen exchange reaction kinetics for cerium(IV) oxide at 1000 °C
Christofer E. Whiting, John M. Douglas, Bethany M. Cremeans, Chadwick D. Barklay and Daniel P. Kramer
page 116

Parameter Tested	Low	High
Isotopic Effects	^{16}O	^{18}O
Sample Size (mg)	5	100
O_2 Partial Pressure (Torr)	116	806
Total Pressure (Torr)	417	1918
a_s ($m^2 * g^{-1}$)	4.23	72.91
Binary Gas Composition	He, Ne, Ar, and N_2	

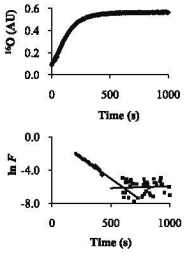

Oxygen exchange kinetics on CeO_2 at 1000 °C are independent of a wide range of experimental conditions and exhibit first-order chemical reaction kinetics

Structural, microstructural and vibrational analyses of the monoclinic tungstate $BiLuWO_6$
H. Ait Ahsaine, A. Taoufyq, L. Patout, M. Ezahri, A. Benlhachemi, B. Bakiz, S. Villain, F. Guinneton and J.-R. Gavarri
page 124

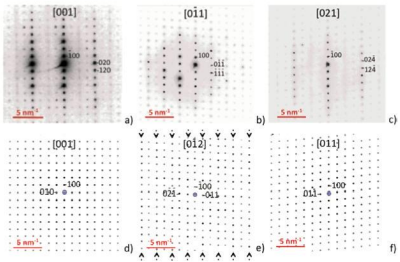

The average structure of $BiLuWO_6$ determined from X-ray diffraction data can be represented by $A2/m$ space group. Experimental Electron Diffraction patterns along the [0vw] zone axes of the monoclinic structure and associated simulated patterns show the existence of a monoclinic superstructure with space group $P2$ or $P2/m$.

Searching for "$LiCr^{II}PO_4$"
E. Mosymow, R. Glaum and R.K. Kremer
page 131

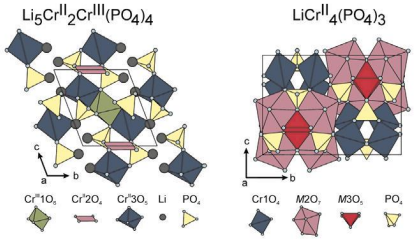

Investigations on the equilibrium relations in the system Li/Cr/P/O revealed the two hitherto unknown phosphates $Li_5Cr^{II}_2Cr^{III}(PO_4)_4$ and $LiCr^{II}_4(PO_4)_3$. They form instead of "$LiCr^{II}PO_4$". The crystal structures, magnetic behavior and optical spectra of these phosphates are reported.

Space formations and nonlinear properties of noncentrosymmetric germanates
Anton Sergeevich Korotkov
page 141

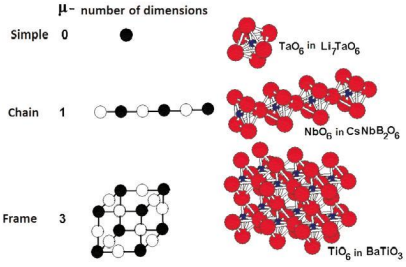

Examples of space formations of polyhedra.

A multi-functional coordination polymer coexisting spontaneous chirality resolution and weak ferromagnetism
Xiu-Hua Li, Qi Zhang and Ping Hu
page 151

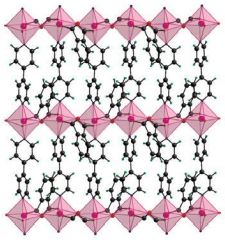

A 2D cobalt coordination polymer compound showing spontaneous chirality resolution and weak ferromagnetism.

Nanostructured gadolinium-doped ceria microsphere synthesis from ion exchange resin: Multi-scale in-situ studies of solid solution formation
Marie Caisso, Florent Lebreton, Denis Horlait, Sébastien Picart, Philippe M. Martin, René Bès, Catherine Renard, Pascal Roussel, Daniel R. Neuville, Kathy Dardenne, Jörg Rothe, Thibaud Delahaye and André Ayral
page 155

The elaboration of micro-spherical precursors leading to the formation of nano-oxide soft agglomerates was studied and approved through the use of ion exchange resin loaded with cerium and gadolinium. The formation of the solid solution was followed through in-situ measurements such as XAS, XRD, Raman, TGA and DSC. Key temperatures were identified for the formation of the mixed-oxide. Following this study, the microstructure and particle size of oxide microspheres formed highlight the formation of soft nano-arrangments.

Spectral characteristics of nanoamorphous phosphors obtained by evaporation of $Sr_2Gd_8(SiO_4)_6O_2$: Eu polycrystals
M.G. Zuev, S.Yu. Sokovnin, V.G. Il'ves, I.V. Baklanova and A.A. Vasin
page 164

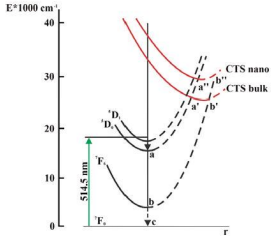

Schematic configurational-coordinate diagram for Eu^{3+} ion in polycrystalline $Sr_2Gd_{6.4}Eu_{1.6}Si_6O_{26-\delta}$ and nanoamorphous phosphor.

Fabrication of graphene/polyaniline composite multilayer films by electrostatic layer-by-layer assembly
Jiaojiao Cong, Yuze Chen, Jing Luo and Xiaoya Liu
page 171

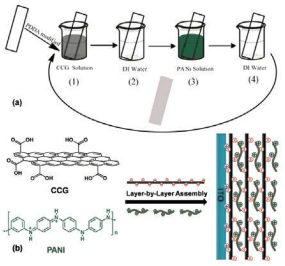

A novel graphene/polyaniline (CCG/PANI) film was prepared by layer-by-layer assembly.

Facile synthesis of hierarchical hollow ε-MnO_2 spheres and their application in supercapacitor electrodes
Dandan Han, Xiaoyan Jing, Pengcheng Xu, Yuansheng Ding and Jingyuan Liu
page 178

The MnO_2 shell with $MnCO_3$ intermediate core is prepared at room temperature; the hollow structure with excellent permeated shell enhanced the discharge capacity and electrochemical stability.

Phase equilibria in the La–Mg–Ge system at 500 °C and crystal structure of the new ternary compounds $La_{11}Mg_2Ge_7$ and $LaMg_{3-x}Ge_2$
S. De Negri, P. Solokha, M. Skrobańska, D.M. Proserpio and A. Saccone
page 184

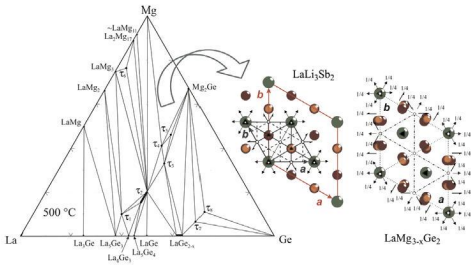

La–Mg–Ge isothermal section at 500 °C and group–subgroup relation between the $LaLi_3Sb_2$ (parent type) and $LaMg_{3-x}Ge_2$ (derivative) structures.

Continued

$Ag_{1.75}InSb_{5.75}Se_{11}$: A new noncentrosymmetric compound with congruent-melting behavior
Wenyu Hao, Yemao Han, Rongjin Huang, Kai Feng, Wenlong Yin, Jiyong Yao and Yicheng Wu
page 196

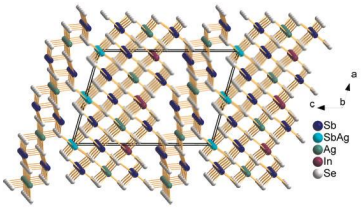

$Ag_{1.75}InSb_{5.75}Se_{11}$ has a new three-dimensional layer structure which consists of infinite $^{2}_{\infty}[AgSb_2Se_4]$ layers and $^{2}_{\infty}[Ag1(Sb6)Ag3InSb_3Se_8]$ layers.

Lanthanide coordination polymers: Synthesis, diverse structure and luminescence properties
Xue-Qin Song, Yao-Kun Lei, Xiao-Run Wang, Meng-Meng Zhao, Yun-Qiao Peng and Guo-Quan Cheng
page 202

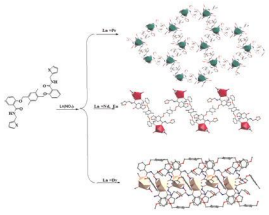

We present herein six lanthanide coordination polymers of a new semirigid *exo*-bidentate ligand which not only display diverse structures but also possess strong luminescence properties.

Hierarchical Na-doped cubic ZrO_2 synthesis by a simple hydrothermal route and its application in biodiesel production
Hugo A. Lara-García, Issis C. Romero-Ibarra and Heriberto Pfeiffer
page 213

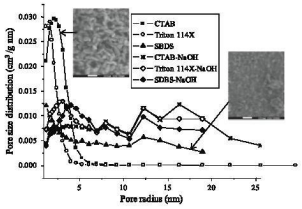

Hierarchical growth of cubic Na-ZrO_2 phase was synthesized by hydrothermal processes in the presence of surfactants and sodium. Sodium addition stabilized the cubic phase by a Na-doping process, while the microstructural characteristics varied with surfactants. Finally, this surface reactivity was evaluated on the biodiesel transesterification reaction.

Structures and thermoelectric properties of double-filled $(Ca_xCe_{1-x})Fe_4Sb_{12}$ skutterudites
Y.G. Yan, W. Wong-Ng, L. Li, I. Levin, J.A. Kaduk, M.R. Suchomel, X. Sun, G.J. Tan and X.F. Tang
page 221

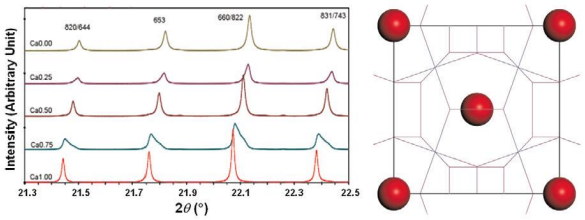

Detailed structural information to correlate with thermoelectric properties in a series of double-filled $(Ca_xCe_{1-x})Fe_4Sb_{12}$ skutterudite samples were obtained using synchrotron X-ray diffraction and first principle calculations.

Rapid Communications

$\{[M(NH_3)_6][Ag_4M_4Sn_3Se_{13}]\}_\infty$ (M=Zn, Mn): Three-dimensional chalcogenide frameworks constructed from quaternary metal selenide clusters with two different transition metals
Wei-Wei Xiong, Jianwei Miao, Pei-Zhou Li, Yanli Zhao, Bin Liu and Qichun Zhang
page 146

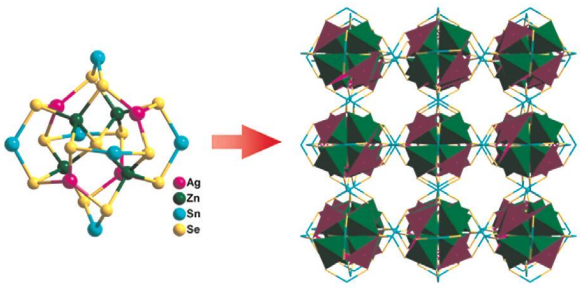

Two 3D framework selenides, $[M(NH_3)_6][Ag_4M_4Sn_3Se_{13}]$ (M=Zn (1), Mn (2)), constructed from quaternary metal selenide clusters, have been solvothermally synthesized and are photoactive under visible light illumination.